catalysts

MDPI

Article

Feasibility Assessment on Remanufacturing of Ni–Mo/γ–Al_2O_3 Catalyst for Residue Hydrodesulfurization

Seon-Yong Ahn [1,†], Woo-Jin Na [2,†], Kyoung-Jin Kim [1], Beom-Jun Kim [1], Hea-Kyung Park [2,*] and Hyun-Seog Roh [1,*]

[1] Department of Environmental and Energy Engineering, Yonsei University, 1 Yonseidae-gil, Wonju 26493, Republic of Korea; syahn99@yonsei.ac.kr (S.-Y.A.); kyoungjinkim@yonsei.ac.kr (K.-J.K.); beomjunkim@yonsei.ac.kr (B.-J.K.)

[2] Department of Materials Science & Chemical Engineering, Hanseo University, 46 Hanseo 1-ro, Heami-myun, Seosan 31962, Republic of Korea; nawoodang@naver.com

* Correspondence: jhkp@hanseo.ac.kr (H.-K.P.); hsroh@yonsei.ac.kr (H.-S.R.)

† These authors contributed equally to this work.

Abstract: Residue hydrodesulfurization (RHDS) is a critical process in the petroleum refining industry for removing sulfur compounds from heavy residual oils. However, catalysts used in RHDS can easily be deactivated by numerous factors, leading to reduced process efficiency and economic benefits. The remanufacturing of spent catalysts can be a useful strategy for extending the lifespan of catalysts, reducing waste, and improving process sustainability. This paper proposes an effective catalyst remanufacturing process for commercial RHDS catalysts. In detail, sequential unit processes including oil washing (OW), complete incineration (CI), and acid leaching (AL) were conducted to remanufacture the spent RHDS catalysts. We also highlight some of the key challenges in remanufacturing catalysts, such as the key factors involved in catalyst deactivation. Finally, we provide future perspectives on the development of an effective catalyst remanufacturing process for RHDS, with the goal of improving the efficiency, sustainability, and competitiveness of the petroleum refining industry.

Keywords: remanufacturing; catalyst; residue hydrodesulfurization; sulfur removal; vanadium removal; petroleum refining

Citation: Ahn, S.-Y.; Na, W.-J.; Kim, K.-J.; Kim, B.-J.; Park, H.-K.; Roh, H.-S. Feasibility Assessment on Remanufacturing of Ni–Mo/γ–Al_2O_3 Catalyst for Residue Hydrodesulfurization. *Catalysts* **2023**, *13*, 738. https://doi.org/10.3390/catal13040738

Academic Editors: Roman G. Kukushkin and Petr M. Yeletsky

Received: 17 March 2023
Revised: 11 April 2023
Accepted: 11 April 2023
Published: 13 April 2023

1. Introduction

Currently, the global consumption of catalysts surpasses 800,000 t/y, with approximately 30% being hydrodesulphurization (HDS) catalysts utilized in the petroleum refining sector [1]. HDS catalysts are mainly employed in the oil refining sector to eliminate sulfur heteroatoms, which in turn, improves the quality of intermediate and final products [2]. In the process of heterogeneous catalysis, compounds with heteroatoms such as Ni and V, as well as polycyclic aromatic hydrocarbons, colloids, and asphaltenes present in crude oil, can be accumulated on the catalyst surface in the form of NiS_x, VS_2, VS_4, coke, and other substances [2]. The accumulation by these metal sulfates and coke deposition induced significant catalyst deactivation [3,4]. Accordingly, the HDS catalysts have a short lifespan of approximately 6–12 months [5]. This is the reason that the amount of spent catalyst discarded from the hydrotreating unit is always greater than the amount of fresh catalyst loaded in the reactor.

The hydroprocessing units in refineries are responsible for a significant portion of spent catalysts due to the substantial use of catalysts in the hydrotreating process, which is utilized to refine and enhance various petroleum streams and residues. In addition, the amount of spent catalysts discharged as solid waste has increased significantly in recent years due to the rapid growth of distillate hydrotreating capacity to meet the growing demand for ultra-low sulfur transportation fuels, the increase in the processing of heavier

feedstocks containing high sulfur and metal content, and the rapid deactivation and unavailability of reactivation processes for residue hydroprocessing catalysts. In addition, as the growth engine for the rebound from the economic recession caused by the COVID-19 pandemic in the last three years is based on fossil fuels, this prospect is expected to continue [6,7]. From an environmental point of view, spent catalysts have been designated as hazardous waste by U.S. Environmental Protection Agency because of their self-heating and toxic nature. Metal components (Co, Ni, V) from the spent catalysts can be leached into water, thereby contaminating the aquatic environment. Additionally, there is a risk of releasing harmful gases such as HCN when spent catalysts with deposited carbon come into contact with water [8]. Therefore, including the above reasons, the strict environmental regulations concerning the handling and disposal of spent catalysts have led to significant interest in the research and development of processes for recycling and reutilizing spent hydrotreating catalysts.

Three methods are generally employed to minimize the amount of spent catalyst: (1) utilizing in less challenging hydrotreating or alternative processes, (2) rejuvenation and regeneration, and (3) decreasing the consumption of catalysts by utilizing improved catalysts with extended lifespans. However, research into the development of new catalysts that outperform commercial catalysts is still in progress. Therefore, research on alternative ways to utilize spent catalysts or reactivate them is currently being actively pursued [9].

Several recent studies have investigated various ways to utilize or regenerate spent hydrotreating catalysts. Srour et al. reported the applicability of the non-thermal plasma regeneration process of the spent $CoMoP/Al_2O_3$ catalyst for HDS. It has been found that, despite the presence of $CoMoO_4$ and other oxide species that impede the promotional role of cobalt, HDS catalysts regenerated through non-thermal plasma exhibit higher hydrogenation activity than those regenerated through conventional thermal means in industrial units [10]. Gao et al. applied a roasted spent HDS ash as a catalytic promoter. Although there is a problem of gaseous pollutants such as S and N being released during the thermal decomposition process, the potential for self-circulation of the spent oily HDS catalyst and value-added energy recovery through thermal cracking has been verified [11]. Yang et al. proposed a microwave pyrolysis method as a strategy for removing oil content from the spent HDS catalyst, and confirmed that it was effective in removing elemental carbon including oil [12]. In addition, various studies have been conducted on the recovery of valuable metals from spent catalysts through leaching [2,13–16]. However, most of the studies have focused only on one process of treating the spent catalyst [17–20], and there have been few studies examining the reusability of the catalyst through remanufacturing.

Overall, the remanufacturing of catalysts for RHDS is an important area of research and development, with potential benefits for improving the efficiency and sustainability of the petroleum refining industry. Further studies are needed to optimize the remanufacturing processes and evaluate their economic and environmental impacts.

In this study, we proposed an effective catalyst remanufacturing process consisting of oil washing (OW), complete incineration (CI), and acid leaching (AL). The physicochemical properties of each catalyst in each unit step were analyzed by various characterization techniques and correlated with their activity results in the HDS of the dibenzothiophene (DBT) reaction.

2. Results and Discussion

2.1. Elemental Composition of the Ni–Mo/γ–Al_2O_3 Catalyst during the Remanufacturing Process

Table 1 summarizes the inductively coupled plasma optical emission spectroscopy (ICP-OES) results of the Ni–Mo/γ–Al_2O_3 (NMA) catalysts in each unit process of catalyst remanufacturing. The NMA – F catalyst, in its freshly purchased state, exhibited the following composition: Ni 3.19%, Mo 8.30%, and Al 45.51%. The NMA – OW, spent catalyst applied to the HDS of heavy oil after washing the oil component, showed a similar content of Ni to NMA – F, but the content of Mo and Al decreased considerably. In addition, it was confirmed that the deposition of V and S contained in the residue proceeded. The

accumulation of vanadium prevents activity recovery by blocking the pore structure and active sites, and sulfur is known as a representative catalyst poison due to its strong adsorption to reactants [21–24]. After complete incineration (NMA – CI), it was confirmed that approximately 87% of the sulfur component was successfully removed as planned in the catalyst remanufacturing process proposed in this study. For the leaching of vanadium remaining after complete incineration, acid leaching (NMA – AL) was performed using oxalic acid solution. It was confirmed that most of the vanadium was removed by showing 0.27 wt.%. However, it was confirmed that Ni (↓ 47%) and Mo (↓ 89%), which can act as active species, also significantly decreased during this process. As a result, vanadium and sulfur corresponding to contaminants were successfully removed through the catalyst remanufacturing process, but Ni and Mo corresponding to active species were also leached.

Table 1. Elemental composition of the Ni–Mo/γ–Al_2O_3 catalysts during the remanufacturing process.

Catalyst	Elemental Composition (wt.%) [a]				
	Ni	**Mo**	**Al**	**V**	**S**
NMA – F	3.19	8.30	45.51	-	-
NMA – OW	3.13	5.24	29.03	1.89	8.46
NMA – CI	4.25	7.20	37.56	2.75	1.08
NMA – AL	2.23	0.79	40.44	0.27	0.32

[a] Determined by ICP-OES.

2.2. Textural Properties of the Ni–Mo/γ–Al_2O_3 Catalyst during the Remanufacturing Process

As mentioned above, it is well known that vanadium and sulfur contained in residue oil affect the pore structure to deactivate the catalyst. Therefore, in this section, the N_2 physisorption results were presented to examine the change in the pore structure by the catalyst remanufacturing process. The textural properties of the catalysts during the remanufacturing process are given in Table 2. The specific surface area (S.A.) decreases after the RHDS reaction. This is due to the pore blocking phenomenon by the accumulation of residual contaminants (V, S, C) [21–23]. The specific surface area of the catalyst was restored to almost the same level as that of the fresh catalyst (NMA – F) after complete incineration (NMA – CI) through the catalyst remanufacturing process consisting of sequential processes of complete incineration and acid leaching. In addition, the specific surface area of NMA – AL, which is treated by acid leaching, showed a higher value than that of NMA – F. As shown in the ICP-OES results, this can be explained by the simultaneous leaching of V and S contaminants as well as active metal components. The total pore volume also showed the same trend as the specific surface area. Figure 1 depicts the N_2 adsorption/desorption isotherms of the catalysts. Catalysts in the entire catalyst remanufacturing process, including the NMA – F catalyst, showed adsorption branches of type IV classified by the International Union of Pure and Applied Chemistry (IUPAC) [25]. These results indicate that all catalysts have mesoporous structures [26–28]. In this case, if the diameter of the pore is wider than 4 nm, then hysteresis will occur alongside capillary condensation. All catalysts except the NMA – OW catalyst showed an H1 hysteresis loop. The presence of the H1 hysteresis loop is indicative of materials with a narrow range of uniform mesopores [25]. On the other hand, the NMA – OW catalyst exhibited an H2 hysteresis loop. Pore structures that are more complex are associated with the H2 hysteresis loop. This phenomenon can be caused by pore blocking [21–23,29]. Since the NMA – OW catalyst is in almost the same state as the catalyst after the RHDS reaction, it can be expected to exhibit such a pore structure for pore blocking by contaminants such as V and S in the residue oil.

Table 2. Textural properties of the Ni–Mo/γ–Al_2O_3 catalysts during the remanufacturing process.

Catalyst	S.A. (m^2/g) [a]	Pore Volume (cm^3/g) [a]	Mean Pore Diameter (nm) [a]	CO Uptake (μmol/g) [b]	Active Sites (10^{18} atoms/g_{cat}) [b]	Metal S.A. (m^2/g) [b]	Mechanical Strength (N/mm^2) [c]
NMA – F	150.5	0.515	10.9	17.2	7.57	8.73	34.7
NMA – OW	42.9	0.142	7.6	1.5	0.69	1.19	23.7
NMA – CI	149.3	0.502	9.1	23.1	10.41	12.46	33.6
NMA – AL	204.2	0.714	9.9	1.6	0.76	3.87	29.6

[a] Estimated from N_2 adsorption at −196 °C. [b] Estimated from CO-chemisorption. [c] Estimated from compression stress at maximum compressive load.

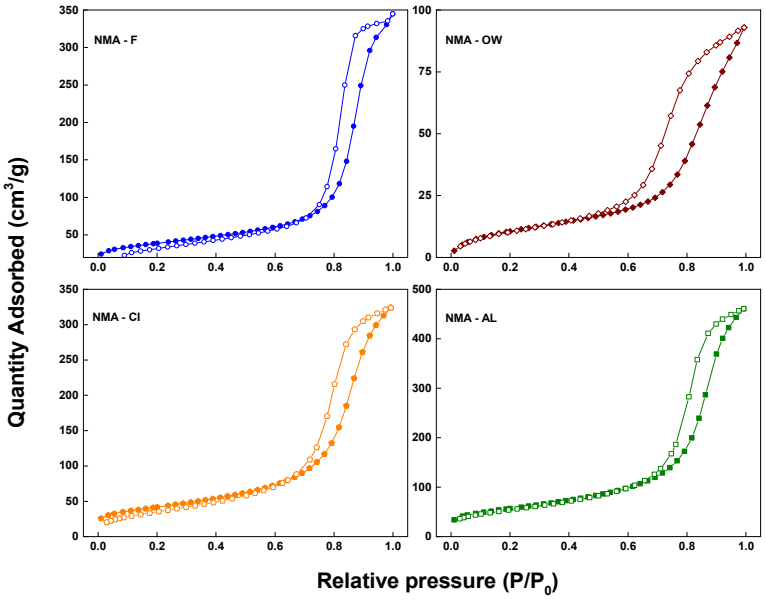

Figure 1. N_2 physisorption isotherm linear plots of the Ni–Mo/γ–Al_2O_3 catalysts during the remanufacturing process (closed symbol: adsorption, open symbol: desorption).

To further investigate the changes in the pore structures during the catalyst remanufacturing process, the pore size distribution was analyzed by the desorption branch using the Barrett-Joyner-Halenda (BJH) theory, as shown in Figure 2 and Table 3. During the catalyst remanufacturing process, the catalysts exhibited uniform pore diameters of 7.6 to 10.9. Notably, the NMA – AL catalyst showed a main pore diameter distribution peak located at 11.2 nm, which is larger than that of the NMA – F catalyst. As revealed in the ICP-OES results, this is because other metals including V were also leached by the acid leaching treatment. This is in agreement with the results reported by Liu et al. [30]. They revealed that the pore volume and average pore diameter decreased as the metal content increased in the NiMo-Al_2O_3 catalyst. In addition, the NMA – OW catalyst showed a main pore diameter distribution peak of 7.1 nm, which is the smallest size. Bore et al. claimed that when metal particles outgrow the pore size, the nearby pore structure can collapse [31,32]. Therefore, it can be seen that the clogging of the pore structure occurred due to complex phenomena, including sintering of the active metal components and deposition of contaminants (V, S, C) present in the reactants during the RHDS reaction. Moreover, disordered accumulation of the active species induced by the reaction temperature of RHDS reaction can be another reason for pore blocking. The resulting collapse of the pore structure due to the low surface area lowers the mass transfer rate and acts as a major cause of catalyst deactivation [33,34]. The results of the metal surface area calculated by CO-chemisorption support this hypothesis. The NMA – OW catalyst exhibited the lowest metal surface area (1.19 m^2/g) among the treated catalysts and increased in the following order: NMA – OW (1.19 m^2/g) < NMA – AL (3.87 m^2/g) < NMA – F (8.73 m^2/g) < NMA – CI (12.46 m^2/g). The number of active sites estimated from the CO uptake shows the same trend with metal

surface area. The lowest value of NMA – OW can be ascribed as the sintering of active species, and is consistent with N_2 physisorption results. Interestingly, NMA – CI showed a higher value than that of NMA – F. This is expected to result from the enhancement of the metal–support interaction due to the additional heat treatment. Additionally, NMA – AL exhibited a value comparable to NMA – OW, despite having a surface area close to five times larger. Generally, a high number of active sites is achieved by a high surface area [35]. In this case, it is determined that sintering occurred due to the metal–support interaction weakened by acid leaching process. Another factor may be sintering caused by a relatively high Ni/Mo ratio, which is due to Mo leaching [36].

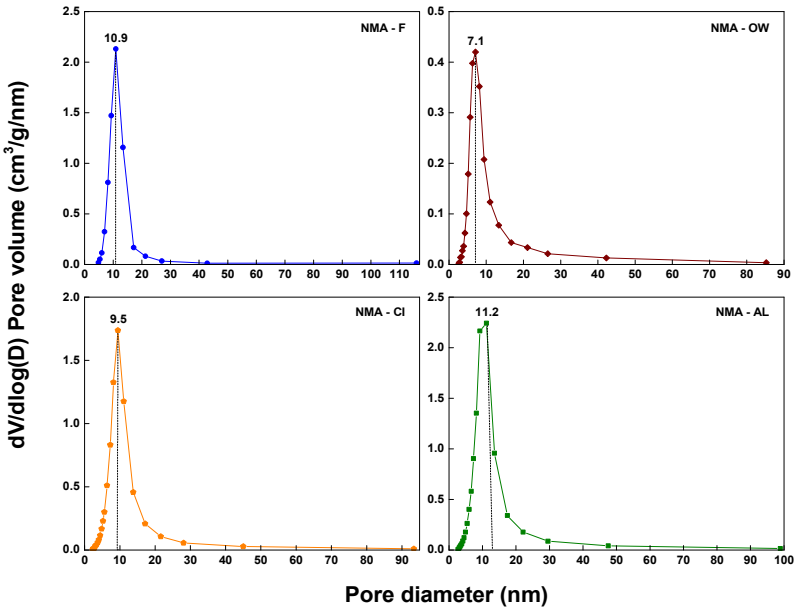

Figure 2. Pore distribution of Ni–Mo/γ–Al_2O_3 catalysts during remanufacturing process.

Table 3. Pore volume distribution of the Ni–Mo/γ–Al_2O_3 catalysts during the remanufacturing process.

Catalyst	Pore Volume (cm^3/g)		
	Micropore (d_p < 2 nm)	Mesopore (2 nm < d_p < 50 nm)	Macropore (d_p > 50 nm)
NMA – F	-	0.499 (97.0%)	0.016 (3.0%)
NMA – OW	-	0.140 (98.4%)	0.002 (1.6%)
NMA – CI	-	0.497 (99.0%)	0.005 (1.0%)
NMA – AL	-	0.707 (99.0%)	0.007 (1.0%)

As a result, most of the textural properties were recovered through the catalyst remanufacturing process, showing about 85% of mechanical strength compared to the fresh catalyst.

2.3. Crystal Structures of the Ni–Mo/γ–Al_2O_3 Catalyst during the Remanufacturing Process

Changes in the crystal structure of the catalyst by the catalyst remanufacturing process were investigated through powder X-ray diffraction (PXRD) analysis, and the results are shown in Figure 3. During the remanufacturing process, no particular crystal structure changes were observed, but some samples showed slight deformation. As shown in Figure 3, all treated catalysts mainly show diffraction peaks characteristic of γ-Al_2O_3 (PDF-ICDD # 29-0063) [37,38]. For all treated catalysts, diffraction peaks corresponding to the Ni and Mo compounds were not detected due to the low content, as confirmed by the ICP-OES results. Compared to other treated catalysts, the NMA – OW catalyst show a characteristic peak corresponding to NiV_2S_4 (PDF-ICDD # 36-1132) at 34.966° [11]. This diffraction peak disappeared after the subsequent remanufacturing process. This result

indicates that the metal contaminants mainly exist in the form of NiV_2S_4 after the RHDS reaction. In addition, in the case of NMA – CI, it was confirmed that the diffraction peaks of MoO_2 (PDF-ICDD # 50-0739) and MoO_3 (PDF-ICDD # 05-0508) were more prominent than those of other treated catalysts [39]. This suggests that MoO_2 and MoO_3 species coexist due to the increase in Mo-Al_2O_3 interaction by additional heat treatment. These peaks disappeared after acid leaching, confirming that the metal–support interaction is weakened by acid leaching. This result is consistent with the CO-chemisorption results.

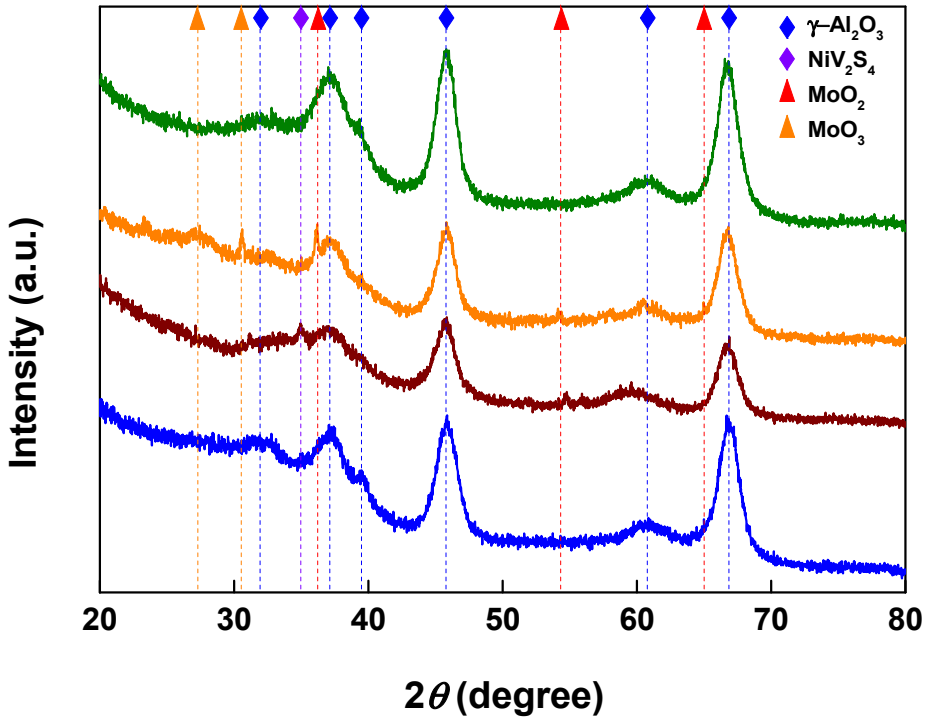

Figure 3. PXRD patterns of the Ni–Mo/γ–Al_2O_3 catalysts during the remanufacturing process.

2.4. Reduction Properties of the Ni–Mo/γ–Al_2O_3 Catalyst during the Remanufacturing Process

As the HDS reaction applies H_2 gas as a co-fed reactant, the reduction property of the applied catalyst can be an important indicator for determining the reaction efficiency. Figure 4 presents H_2-temperature programmed reduction (H_2-TPR) results of catalysts during remanufacturing process. All treated catalysts exhibited two reduction peaks at 400 °C and 800 °C, respectively. Generally, reduction of MoO_3 has two sequential steps: $MoO_3 \rightarrow MoO_2 \rightarrow Mo$. The first low reduction peak ascribed the transformation of the polymeric octahedral Mo species from Mo^{6+} to Mo^{4+} [40,41]. This kind of Mo has amorphous structure, and is a high defect multilayer Mo oxide or heteropoly acid. This octahedral Mo is considered as active precursor in the HDS reaction [42]. The second high temperature reduction peak indicates the reduction of the polymeric octahedral Mo^{4+} and intensive reduction of the tetrahedral Mo species [43,44]. This type of Mo is highly dispersed Mo and MoO_3. Mo^{4+} species has a negative effect on sustainability for the Ni-Mo-S phase [45]. In particular, the first reduction peak of NMA – OW shifted to a lower temperature range. This is due to the enhanced reducibility by the additional reduction of the sulfur compounds present in the spent catalyst, which is consistent with the result of Liu et al. [46]. In addition, it can be seen that the Mo^{4+} reduction peak near 800 °C is also rarely observed, and the metal–support interaction has been weakened due to the improved reducibility. On the other hand, after the complete incineration, the first reduction peak shifted to a high temperature and a new reduction peak was observed at 500 °C. The H_2 consumption peak at 500 °C is known to be due to the reduction of $NiMoO_4$ [47,48]. In addition, the intensity of the reduction peak corresponding to Mo^{4+} was also emphasized.

It suggests that the strong metal to support interaction (SMSI) of the catalyst is promoted by the complete incineration process. This result is well matched with the CO-chemisorption and PXRD analysis results. After the acid leaching process, the H_2 consumption of all reduction peaks was reduced. This is the result of an additional metal (Ni, Mo) leaching and is consistent with the results of ICP-OES and CO-chemisorption.

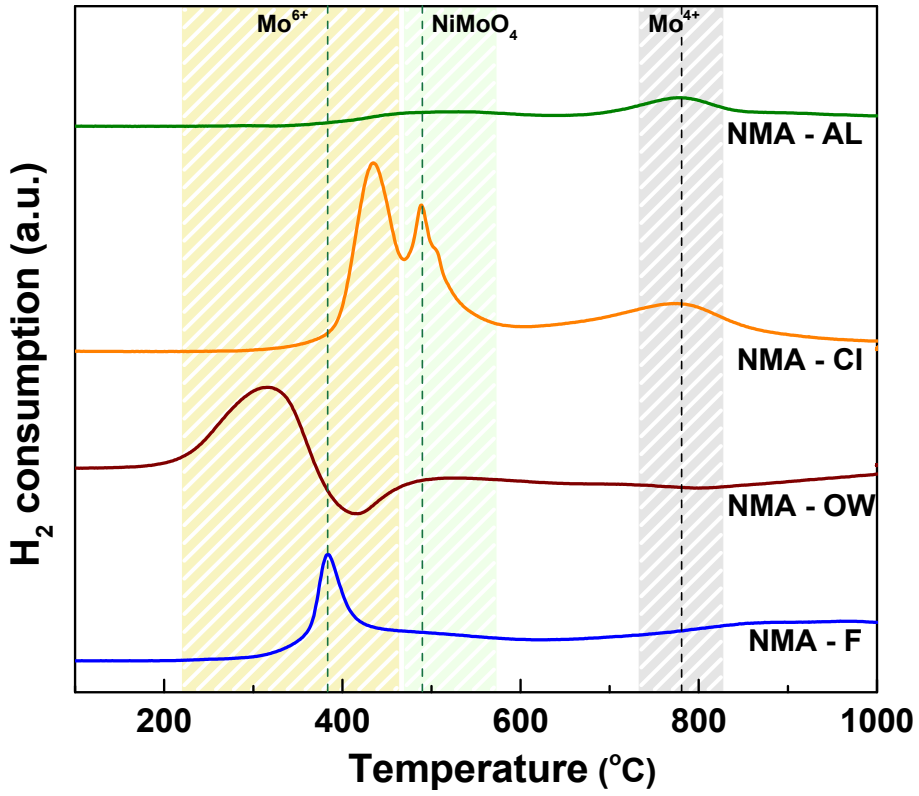

Figure 4. TPR patterns of the Ni–Mo/γ–Al_2O_3 catalysts during the remanufacturing process.

2.5. FT-IR Analysis of the Ni–Mo/γ–Al_2O_3 Catalyst during the Remanufacturing Process

In order to clarify the structural changes and residual contents during the catalyst remanufacturing process, Fourier-transform infrared spectroscopy (FT-IR) spectra of the Ni–Mo/γ–Al_2O_3 catalysts during the remanufacturing process were collected in the range of 1000–4000 cm^{-1}. According to the results presented in Figure 5, all treated catalysts exhibit the broad absorption band located at 3433 cm^{-1} and an absorption band with low intensity located at 1630 cm^{-1}, which are due to the stretching vibration of the O-H bond and the bending vibration of the H-O-H bond of the adsorbed H_2O molecule, respectively [49]. These absorption bands indicate that H_2O molecules are linked to nanoparticles in the treated catalysts. The NMA – OW catalyst exhibited a slightly different spectrum compared to other catalysts. In particular, the absorption bands located at 1400, 1450, and 2924 cm^{-1} were further detected. These peaks correspond to branched-chain and cyclic paraffin (1400 cm^{-1}), straight chain olefins (1450 cm^{-1}), and the C-H bond of organic residues (2924 cm^{-1}), respectively. It also showed a distinct absorption band located at 1088 cm^{-1} corresponding to the asymmetrical and symmetrical C-O-C ring stretching vibration. These findings confirm that residual heavy oil components resulting from the RHDS reaction remained in the spent catalyst [50–52]. Catalysts from the subsequent sequential remanufacturing process did not show an absorption band for heavy oil-containing materials. Therefore, it was confirmed that the impurities were successfully removed through the proposed remanufacturing process in this study.

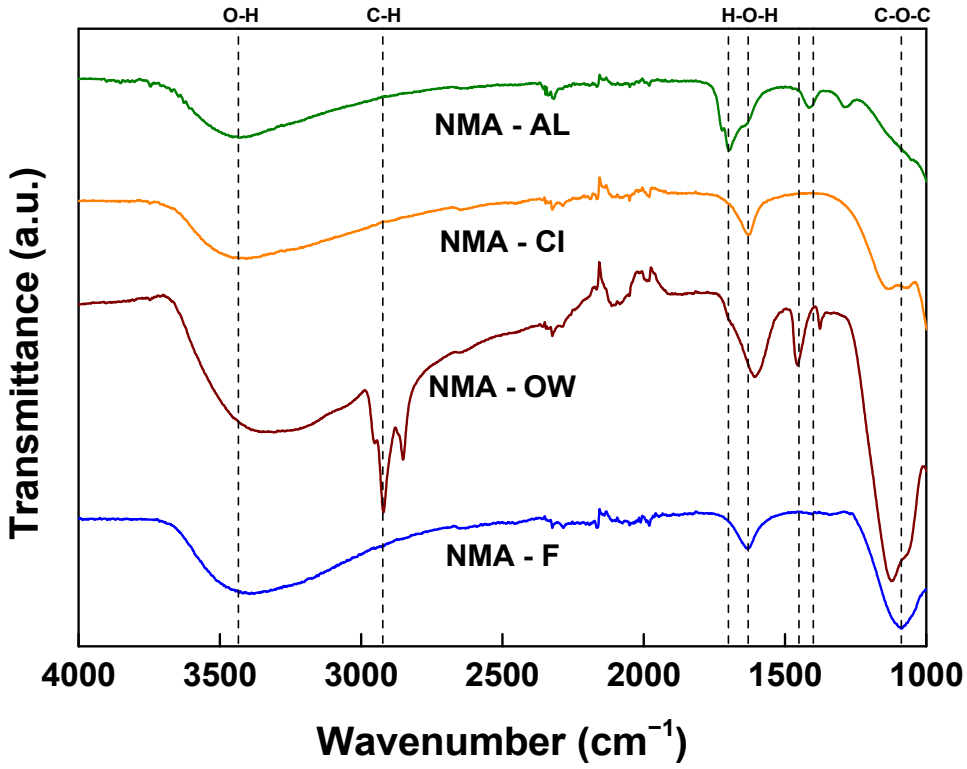

Figure 5. FT-IR spectra of the Ni–Mo/γ–Al_2O_3 catalysts during the remanufacturing process.

2.6. Quantitative Investigation of Impurities in the Ni–Mo/γ–Al_2O_3 Catalyst during the Remanufacturing Process

A quantitative investigation of impurities in the Ni–Mo/γ–Al_2O_3 catalyst during the remanufacturing process was achieved through thermogravimetric analysis (TGA). Figure 6 depicts the TG weight loss curves as a function of temperature for catalysts for each remanufacturing process. The weight loss in the first region corresponding to the temperature range of 20–200 °C is due to residual moisture. The weight loss in the second region, corresponding to the temperature range of 200–400 °C, is attributed to the devolatilization of residual oil components. Accordingly, the spent catalyst (NMA – OW) showed the largest weight loss. It is well known that the weight loss observed after 400 °C is caused by the deposited coke and decomposable inorganic compounds, such as sulfates [37]. The weight loss that occurs after 600 °C is due to heavier carbon deposition and sulfate decomposition. The deposition of coke is usually associated with the diffusion length that reactants and products must cover within the porous catalysts. If the diffusion length is longer, it can result in the generation of more coke, which may be of a heavier type [53]. For the above reasons, the weight loss in the temperature range of 400–1100 °C was set as a value for quantitative investigation of impurities. The weight loss by carbon- and sulfur-containing compounds decreased in the following order: NMA – OW (23%) > NMA – CI (8%) > NMA – AL (4%). This result can be explained by the recovery of the pore structure through the remanufacturing process revealed by the N_2 physisorption analysis. In addition, it is consistent with the FT-IR and ICP-OES results, confirming that impurities are removed by the remanufacturing process.

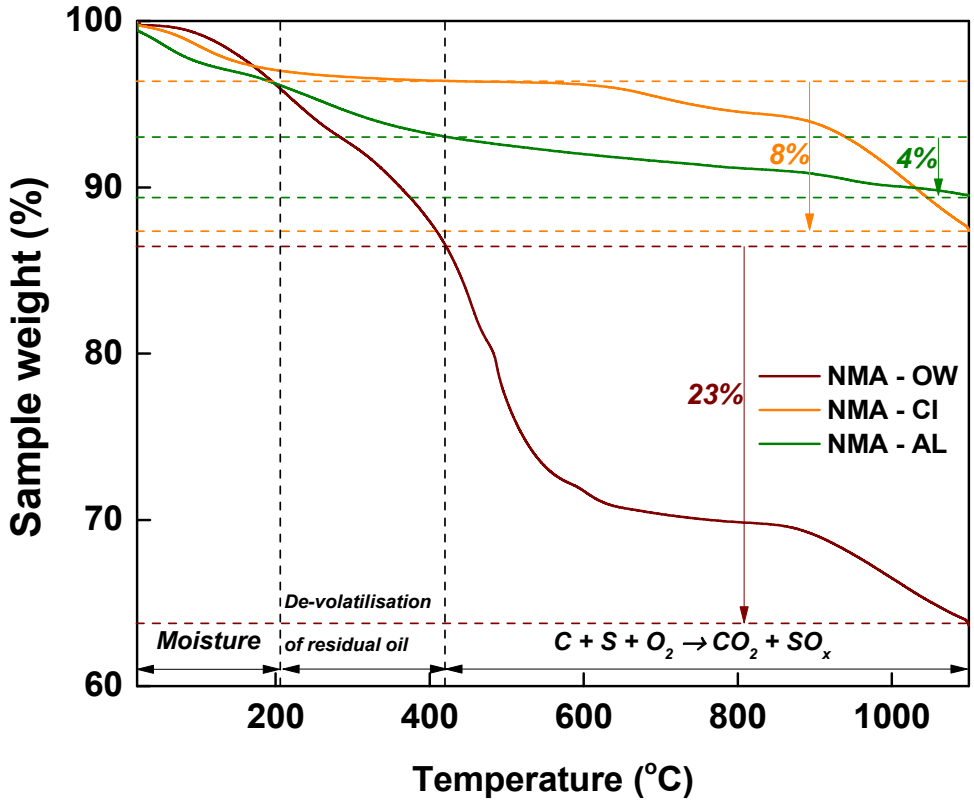

Figure 6. TGA results of the Ni–Mo/γ–Al_2O_3 catalysts during the remanufacturing process.

2.7. HDS Activity Test for the Remanufactured Ni–Mo/γ–Al_2O_3 Catalyst

In order to examine the reusability of the remanufactured catalyst, fresh (NMA – F), spent (NMA – OW), and remanufactured catalysts (NMA – AL) were applied to the HDS of DBT, and their performance was compared and evaluated at the liquid hourly space velocity (LHSV) of 50 h^{-1}. The results are presented in Figure 7 and Table 4. Figure 7A illustrates the DBT conversion as a function of the reaction temperature from 350 to 395 °C. The catalytic activity decreased by approximately 35–40% when the spent catalyst was reused in the HDS of the DBT reaction. Compared to the spent catalyst, the remanufactured catalyst demonstrated an approximately 10% improvement in catalytic activity. The reaction rate and HDS kinetic constant exhibited a similar trend to that of DBT conversion and decreased in the following order: NMA – F (6.37 $\mu mol_{DBT}/g_{cat}{\cdot}s$, 14.3 × 10^{-7} mol/g·s) > NMA – AL (4.59 $\mu mol_{DBT}/g_{cat}{\cdot}s$, 4.3 × 10^{-7} mol/g·s) > NMA – OW (4.06 $\mu mol_{DBT}/g_{cat}{\cdot}s$, 3.4 × 10^{-7} mol/g·s). For an in-depth investigation of the recovery of catalytic activity by the remanufacturing process, turnover frequency (TOF) results were obtained from CO-chemisorption and the apparent activation energies (E_a) were calculated from the Arrhenius equation plot, as shown in Figure 7C. The remanufactured catalyst exhibited a higher TOF value compared to the spent catalyst, even though it had a greater number of active sites. To the contrary, the remanufactured catalyst exhibited a higher apparent activation energy compared to the spent catalyst. This result indicates that the capacity for activity recovery is dependent on the performance of a single active site and the number of active sites. It is noteworthy that the NMA – AL catalyst has a higher number of active sites compared to the NMA – OW catalyst, even though the content of active species identified from ICP-OES is absolutely low.

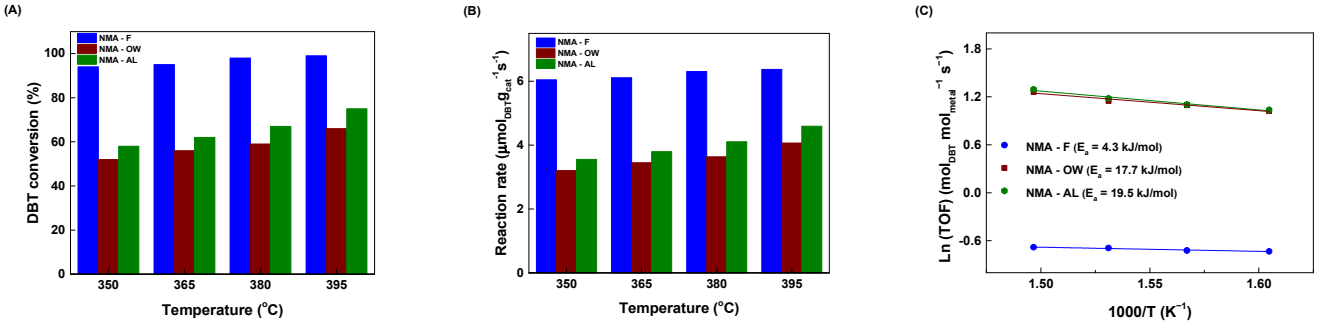

Figure 7. Reaction results of the Ni–Mo/γ–Al_2O_3 catalysts during the remanufacturing process (T = 395 °C, p = 30 bar, LHSV = 50 h^{-1}): (**A**) DBT conversion, (**B**) reaction rate, and (**C**) Arrhenius plots of turnover frequency.

Table 4. Catalytic performance of DBT HDS over Ni–Mo/γ–Al_2O_3 catalysts during the remanufacturing process.

Catalyst	Active Sites (10^{18} atoms/g_{cat})	DBT Conversion (%) [a]	Reaction Rate ($\mu mol_{DBT}/g_{cat}\cdot s$) [a]	TOF (s^{-1}) [a]	E_a (kJ/mol)	HDS Kinetic Constant $\times 10^{-7}$ (mol/g·s) [a]
NMA – F	7.57	99	6.37	0.51	4.3	14.3
NMA – OW	0.69	66	4.06	3.53	17.7	3.4
NMA – AL	0.76	75	4.59	3.65	19.5	4.3

[a] T = 395 °C, p = 30 bar, LHSV = 50 h^{-1}.

This simultaneous improvement in the number of active sites and the TOF value can be explained by enhanced mechanical properties such as pore diameter and mechanical strength. As shown in Figure 8A,B, the DBT conversion increased linearly with the mean pore diameter and mechanical strength. In addition, this tendency appeared more prominent as the reaction temperature increased. As discussed above, it is possible to recover the pore structure that can come into contact with the reactants through the removal of impurities blocking the pore structure of the catalyst. The enhanced specific surface area has the advantage of lowering the diffusion length and thus limiting the potential for carbon deposition. The greater the specific surface area of a catalyst, the more active sites are available to react with the reactants, which generally results in improved catalytic performance [54]. This may be the reason for having a high number of active sites despite the absolutely low content of active species. In addition, the acquisition of SMSI by additional heat treatment (complete incineration) played an additional role in obtaining a high number of active sites. Figure 8C,D shows the DBT conversion according to the residual vanadium and sulfur content. As expected, these results showed a similar trend to the relationship between mechanical properties and DBT conversion. In summary, impurities such as V, S, and C were successfully removed through the catalyst remanufacturing process to secure improved mechanical properties, and the number of active sites and performance per active site were improved by securing SMSI through additional heat treatment.

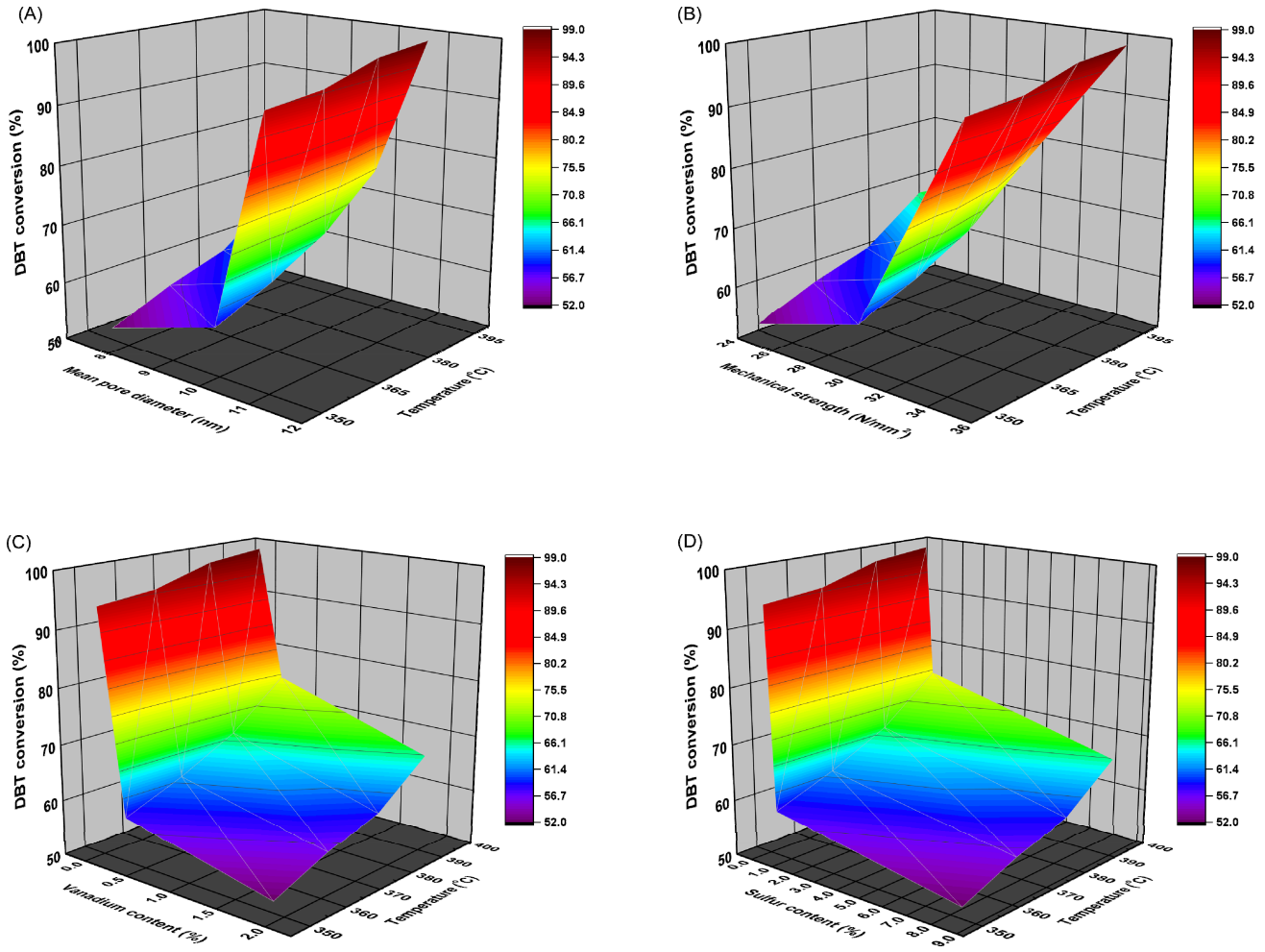

Figure 8. Relationship between DBT conversion and various factors over Ni–Mo/γ–Al_2O_3 catalysts during the remanufacturing process (T = 395 °C, p = 30 bar, LHSV = 50 h^{-1}): (**A**) Mean pore diameter, (**B**) mechanical strength, (**C**) residual V content, and (**D**) residual S content.

3. Materials and Methods

3.1. Catalyst

To confirm the degree of catalyst activity recovery by the catalyst remanufacturing process, a Ni–Mo/γ–Al_2O_3 catalyst purchased from Advanced Refining Technologies LLC (Richmond, California, United States) was used. The catalysts were labeled according to the remanufacturing process as follows: NMA – F (fresh catalyst), NMA – OW (spent catalyst washed by n-heptane), NMA – CI (catalyst after complete incineration), and NMA – AL (remanufactured catalyst with acid leaching as the final process). The elemental composition of the catalyst during the remanufacturing process was analyzed using ICP-OES, and the results are shown in Table 1.

3.2. Catalyst Remanufacturing Process

A series of processes for remanufacturing the Ni–Mo/γ–Al_2O_3 catalyst is shown in Scheme 1. Detailed experimental conditions and information for each process are provided in the following sections.

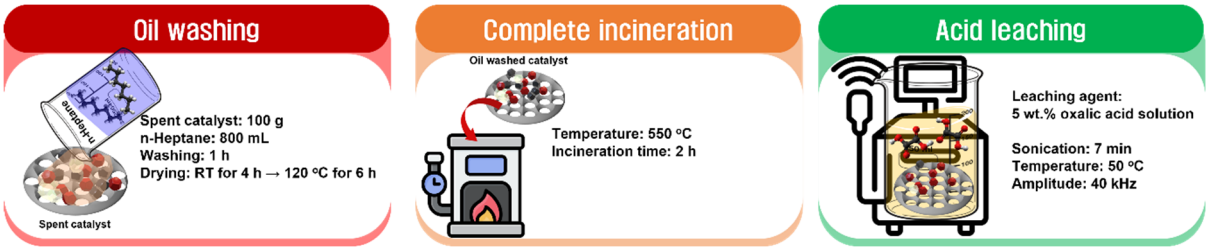

Scheme 1. Catalyst remanufacturing process of the spent Ni–Mo/γ–Al_2O_3 catalysts.

3.2.1. Oil Washing

To remove residual oil components contained in the spent catalyst, 100 g of spent catalyst after HDS of heavy oil was washed with 800 mL of n-heptane (98%, DAEJUNG CHEMICALS & METALS, Siheung-si, Republic of Korea). Oil washing treatment was performed for 1 h. Then, the washed spent catalyst was naturally dried in an atmosphere of room temperature and 1 atm for 4 h. Finally, a drying process was performed in a drying oven at 120 °C for 6 h to remove all residual solvents.

3.2.2. Complete Incineration

After residual oil component removal treatment, the catalyst was roasted at 550 °C for 2 h in contact with air using an aspirator. Inside the roasting furnace, 4 trays for mounting catalysts were installed, and metal foam was cut and applied as a mesh network for stable loading of catalysts.

3.2.3. Acid Leaching

Acid leaching was performed using an aqueous solution of 5 wt.% oxalic acid (98%, Sigma–Aldrich, St. Louis, MI, USA) to remove vanadium-containing materials present in the spent catalyst, which had undergone sequential treatments of oil washing and complete incineration. A suspension of a mixture of 5 wt.% oxalic acid aqueous solution and spent catalyst was sonicated for 7 min at 50 °C at an amplitude of 40 kHz. Then, the resulting catalyst in suspension was washed several times with deionized water and dried at 150 °C for 2 h.

3.3. Catalyst Characterization

The elemental composition of each catalyst in each unit step of remanufacturing was determined by ICP-OES using PerkinElmer Optima 5300 DV equipment (PerkinElmer, Waltham, MA, USA).

The textural properties of the catalysts during the remanufacturing process were analyzed by N_2 physisorption isotherms at −196 °C using an ASAP 2010 apparatus (Micromeritics, Norcross, GA, USA). To eliminate the contaminants and remaining gaseous components from the sample, the samples were subjected to a degassing process for 12 h at a temperature of 110 °C under a vacuum of less than 0.5 mmHg.

CO-chemisorption was conducted using an Autochem II 2920 (Micromeritics, Norcross, GA, USA) apparatus. Prior to the analysis, 0.1 g of the sample was in situ reduced in a 5% H_2/Ar atmosphere at 395 °C for 1 h and then cooled to 60 °C in an Ar atmosphere. Next, CO pulses with 10% CO/He were introduced onto the catalyst surface until the catalyst reached its saturation point with CO. CO uptake was estimated using a thermal conductivity detector and utilized for the determination of active metal dispersion.

PXRD measurements were conducted using a Rigaku Ultima IV (Ni filtered Cu–Kα radiation, 40 kV, 40 mA, Rigaku, The Woodlands, TX, USA) instrument with a scanning resolution of 0.02°.

To examine the reduction properties of the catalysts during the remanufacturing process, H_2-TPR was conducted at 25 °C up to 1000 °C at 10 °C/min in a 10% H_2/Ar atmosphere using an Autochem II 2920 (Micromeritics) instrument.

FT-IR spectra were obtained using a PerkinElmer L1600300 Spectrum Two LiTa (PerkinElmer, Waltham, MA, USA) in the range of 650–4000 cm^{-1} with 1 cm^{-1} resolution.

The quantitative analysis of carbon deposition and residual sulfur containing components on the catalyst was conducted with a thermogravimetry analyzer (TGA, Hitachi STA 7300, Minato City, Tokyo, Japan). The catalyst sample of 5–10 mg was heated from 25 to 1100 °C with a heating rate of 10 °C/min in an air atmosphere.

The mechanical strength of each catalyst in each unit step of the remanufacturing was confirmed through compression stress at maximum compressive load using an Instron 5848 (INSTRON, Norwood, MA, USA) instrument.

3.4. HDS Performance Test

The lab-scale HDS of DBT reaction was performed using a micro-pilot CATATEST UNIT I (O.D.: 19 mm, UtoEngineering, Namyangju-si, Republic of Korea) under a pressure of 30 bar. To simulate crude oil containing sulfur compounds, the reactant feed was prepared by dissolving 0.5 wt.% DBT (98%, Alfa–Aesar, Haverhill, MA, USA) in n-heptane (98%, DAEJUNG CHEMICALS & METALS, Siheung-si, Republic of Korea). For HDS activity tests, 200 mg of commercial Ni–Mo/γ–Al_2O_3 catalyst from each remanufacturing unit process was loaded on the catalyst bed, and a K-type thermocouple was set in the middle of the catalyst bed to monitor the actual reaction temperature. The catalyst was physically mixed with an Al_2O_3 ball (18 mesh, Hankook Ceratec, Daejeon-si, Republic of Korea) at an Al_2O_3 ball/catalyst ratio of 5 (wt/wt). The flow rates of H_2 gas (99.0%) and reactants were set to 834 mL/min and 1.67 mL/min, respectively. The HDS of DBT activity of the catalysts was evaluated at an LHSV of 50 h^{-1} and a temperature range of 350–395 °C. The reaction products were analyzed by on-line gas chromatography (Agilent 7890A, Agilent, Santa Clara, CA, USA) with a DB-17MS capillary column (30 m × 0.25 mm, 0.25 μm, Agilent) equipped with a flame ionized detector (FID). The calculation of DBT conversion was performed using the equations below:

$$\text{DBT conversion}(\%) = \frac{[\text{DBT}]_{\text{in}} - [\text{DBT}]_{\text{out}}}{[\text{DBT}]_{\text{in}}} \times 100$$

For the kinetic analysis, the first-order rate constant was determined using the following equation [10,49,55]:

$$\text{HDS kinetic constant}(\text{k}) = \frac{F}{m}\ln\left(\frac{1}{1-x}\right)$$

The calculation of the TOF was performed using the equation below:

$$\text{TOF} = \frac{([\text{DBT}]_{\text{in}} - [\text{DBT}]_{\text{out}})AS_M F}{D_M W X_M}$$

where $[\text{DBT}]_{\text{in}}$ and $[\text{DBT}]_{\text{out}}$ are the inlet and outlet concentrations of DBT, respectively; F is the molar flow rate of feedstock excluding H_2 ($mol \cdot s^{-1}$); m represents the loading amount of catalyst (g); x is the DBT conversion (%); AS_M is the molar mass of active species; F is the total flow rate ($mol \cdot s^{-1}$); D_M is the dispersion of active species; W is the mass of catalyst (g_{cat}); and X_M is the content of active species ($g_M \cdot {g_{cat}}^{-1}$).

4. Conclusions

We examined the feasibility of the remanufacturing process for spent heavy oil desulfurization catalysts, which are currently being pulverized for the recovery of valuable metals or landfilled as designated wastes in case of low economic feasibility. It was confirmed that catalyst deactivation factors such as vanadium, sulfur, and carbon-containing materials can be effectively removed through the remanufacturing process. The largest deactivation factor of the RHDS catalyst was the deformation of the pore structure by contaminants and the reduction of the specific surface area. When the contaminants in the pores were effectively

removed through the remanufacturing process, it was confirmed that approximately 75% of the activity was recovered compared to the fresh catalyst at a reaction temperature of 395 °C. Above all, the HDS activity was recovered even though most of the catalytic active species were removed by acid leaching, and it was revealed that the most important factor for the RHDS reaction was the mechanical properties (mean pore diameter and mechanical strength) of the catalyst. It is believed that a remanufactured catalyst with performance equivalent to that of the fresh catalyst can be made through research optimization of the remanufacturing process.

Author Contributions: Writing—original draft, S.-Y.A.; writing—review and editing, S.-Y.A. and W.-J.N.; conceptualization, S.-Y.A., W.-J.N., and H.-K.P.; data curation, W.-J.N. and B.-J.K.; investigation, W.-J.N., K.-J.K., and B.-J.K.; visualization, S.-Y.A. and K.-J.K.; funding acquisition, H.-S.R. and H.-K.P.; project administration, H.-K.P.; supervision, H.-K.P. and H.-S.R. S.-Y.A. and W.-J.N. contributed equally to this work. All authors have read and agreed to the published version of the manuscript.

Funding: This work was supported by the Korea Institute of Energy Technology Evaluation and Planning (KETEP) and the Ministry of Trade, Industry and Energy (MOTIE) of the Republic of Korea (No. 20228A10100060).

Data Availability Statement: Data sharing is not applicable to this article.

Conflicts of Interest: The authors declare no conflict of interest.

References

1. Akcil, A.; Vegliò, F.; Ferella, F.; Okudan, M.D.; Tuncuk, A. A review of metal recovery from spent petroleum catalysts and ash. *Waste Manag.* **2015**, *45*, 420–433. [CrossRef]
2. Chen, B.; Du, H.; Guo, Y.; Wang, S.; Peng, J.; Zhang, Y.; Li, L.; Xu, C. Recovering valuable metals from spent hydrodesulfurization catalysts by co-leaching, dissociation, and stepwise precipitation. *J. Environ. Chem. Eng.* **2023**, *11*, 109365. [CrossRef]
3. Ahn, S.Y.; Jang, W.J.; Shim, J.O.; Jeon, B.H.; Roh, H.S. CeO_2-based oxygen storage capacity materials in environmental and energy catalysis for carbon neutrality: Extended application and key catalytic properties. *Catal. Rev.-Sci. Eng.* **2023**, 1–84. [CrossRef]
4. Shafiq, I.; Shafique, S.; Akhter, P.; Yang, W.; Hussain, M. Recent developments in alumina supported hydrodesulfurization catalysts for the production of sulfur-free refinery products: A technical review. *Catal. Rev.-Sci. Eng.* **2022**, *64*, 1–86. [CrossRef]
5. Al-Sheeha, H.; Marafi, M.; Raghavan, V.; Rana, M.S. Recycling and recovery routes for spent hydroprocessing catalyst waste. *Ind. Eng. Chem. Res.* **2013**, *52*, 12794–12801. [CrossRef]
6. IEA. *Global Energy Review 2021*; IEAL: Paris, France, 2021.
7. Lee, Y.L.; Kim, K.J.; Hong, G.R.; Roh, H.S. Target-oriented water–gas shift reactions with customized reaction conditions and catalysts. *Chem. Eng. J.* **2023**, *458*, 141422. [CrossRef]
8. Marafi, M.; Stanislaus, A. Spent catalyst waste management: A review, Part I-Developments in hydroprocessing catalyst waste reduction and use. *Resour. Conserv. Recycl.* **2008**, *52*, 859–873. [CrossRef]
9. Li, L.; Ju, F.; Ling, H. Reactivation of $NiSO_4$/ZnO-Al_2O_3-SiO_2 adsorbent for reactive adsorption desulfurization. *Fuel* **2023**, *339*, 127411. [CrossRef]
10. Srour, H.; Devers, E.; Mekki-Berrada, A.; Toufaily, J.; Hamieh, T.; Batiot-Dupeyrat, C.; Pinard, L. Regeneration of an aged hydrodesulfurization catalyst: Conventional thermal vs non-thermal plasma technology. *Fuel* **2021**, *306*, 121674. [CrossRef]
11. Gao, J.; Cao, Y.; Wu, T.; Li, Y. Self-circulation of oily spent hydrodesulphurization (HDS) catalyst by catalytic pyrolysis for high quality oil recovery. *Environ. Res.* **2023**, *222*, 115359. [CrossRef]
12. Yang, C.; Zhang, J.; Chen, Y.; Wang, C. Efficient removal of oil from spent hydrodesulphurization catalysts using microwave pyrolysis method. *J. Anal. Appl. Pyrolysis.* **2018**, *135*, 169–175. [CrossRef]
13. Liang, X.; Tang, J.; Li, L.; Wu, Y.; Sun, Y. A review of metallurgical processes and purification techniques for recovering Mo, V, Ni, Co, Al from spent catalysts. *J. Clean. Prod.* **2022**, *376*, 134108. [CrossRef]
14. Wang, W.; Zhang, L.; Han, Y.; Zhang, Y.; Liu, X.; Xu, S. Cleaner recycling of spent Ni–Mo/γ-Al_2O_3 catalyst based on mineral phase reconstruction. *J. Clean. Prod.* **2019**, *232*, 266–273. [CrossRef]
15. TENG, Q.; YANG, Z.C.; WANG, H.J. Recovery of vanadium and nickel from spent-residue oil hydrotreating catalyst by direct acid leaching-solvent extraction. *Trans. Nonferrous Met. Soc. China* **2023**, *33*, 325–336. [CrossRef]
16. Xie, Y.; Zhao, S.; Wang, M.; Zhang, G.; Li, Q.; Cao, Z.; Guan, W.; Wu, S. A Novel Technology of Molybdenum Extraction from Spent HDS Catalysts. *J. Sustain. Metall.* **2022**, *8*, 994–1000. [CrossRef]
17. Humadi, J.I.; Nawaf, A.T.; Jarullah, A.T.; Ahmed, M.A.; Hameed, S.A.; Mujtaba, I.M. Design of new nano-catalysts and digital basket reactor for oxidative desulfurization of fuel: Experiments and modelling. *Chem. Eng. Res. Des.* **2023**, *190*, 634–650. [CrossRef]
18. Tang, Y.; Li, S.; Qi, Y.; Yang, S.; Zhou, Q.; Zhang, R.; Qian, B.; Su, B.; Zhang, L.; Dai, B. Coke evolution during the air- and oxy-firing regeneration of a spent Ni/ZnO sulfur adsorbent. *J. Environ. Chem. Eng.* **2023**, *11*, 109455. [CrossRef]

19. Gao, J.; Hao, M.; Wu, T.; Li, Y. A fast and efficient method for the efficient recovery of crude oil from spent hydrodesulphurization catalyst. *Colloids Surfaces A Physicochem. Eng. Asp.* **2022**, *642*, 128650. [CrossRef]
20. Zhang, J.; Yang, C.; Chen, Y.; Wang, C. Efficient Phase Transformation of γ-Al 2 O 3 to α-Al 2 O 3 in Spent Hydrodesulphurization Catalyst by Microwave Roasting Method. *Ind. Eng. Chem. Res.* **2019**, *58*, 1495–1501. [CrossRef]
21. Morales, F.J.; Ancheyta, J.; Torres, P.; Alonso, F. Experimental methodologies to perform accelerated deactivation studies of hydrotreating catalysts. *Fuel* **2023**, *332*, 126074. [CrossRef]
22. Zhu, H.; Mao, Z.; Liu, B.; Yang, T.; Feng, X.; Jin, H.; Peng, C.; Yang, C.; Wang, J.; Fang, X. Regulating catalyst morphology to boost the stability of Ni–Mo/Al_2O_3 catalyst for ebullated-bed residue hydrotreating. *Green Energy Environ.* **2021**, *6*, 283–290. [CrossRef]
23. Iwamoto, R. Regeneration of residue hydrodesulfurization catalyst. *J. Japan Pet. Inst.* **2013**, *56*, 109–121. [CrossRef]
24. Lee, Y.L.; Kim, K.J.; Hong, G.R.; Ahn, S.Y.; Kim, B.J.; Park, H.R.; Yun, S.J.; Bae, J.W.; Jeon, B.H.; Roh, H.S. Sulfur-Tolerant Pt/CeO_2Catalyst with Enhanced Oxygen Storage Capacity by Controlling the Pt Content for the Waste-to-Hydrogen Processes. *ACS Sustain. Chem. Eng.* **2021**, *9*, 15287–15293. [CrossRef]
25. Thommes, M.; Kaneko, K.; Neimark, A.V.; Olivier, J.P.; Rodriguez-Reinoso, F.; Rouquerol, J.; Sing, K.S.W. Physisorption of gases, with special reference to the evaluation of surface area and pore size distribution (IUPAC Technical Report). *Pure Appl. Chem.* **2015**, *87*, 1051–1069. [CrossRef]
26. Lowell, S.; Shields, J.E.; Thomas, M.A.; Thommes, M. *Characterization of Porous Solids and Powders: Surface Area, Pore Size and Density*, 1st ed.; Springer Science & Business Media: Berlin, Germany, 2006.
27. Thommes, M.; Cychosz, K.A. Physical adsorption characterization of nanoporous materials: Progress and challenges. *Adsorption* **2014**, *20*, 233–250. [CrossRef]
28. Landers, J.; Gor, G.Y.; Neimark, A.V. Density functional theory methods for characterization of porous materials. *Colloids Surfaces A Physicochem. Eng. Asp.* **2013**, *437*, 3–32. [CrossRef]
29. Soni, K.; Rana, B.S.; Sinha, A.K.; Bhaumik, A.; Nandi, M.; Kumar, M.; Dhar, G.M. 3-D ordered mesoporous KIT-6 support for effective hydrodesulfurization catalysts. *Appl. Catal. B Environ.* **2009**, *90*, 55–63. [CrossRef]
30. Liu, H.; Li, Y.; Yin, C.; Wu, Y.; Chai, Y.; Dong, D.; Li, X.; Liu, C. One-pot synthesis of ordered mesoporous NiMo-Al_2O_3 catalysts for dibenzothiophene hydrodesulfurization. *Appl. Catal. B Environ.* **2016**, *198*, 493–507. [CrossRef]
31. Jang, W.J.; Kim, H.M.; Shim, J.O.; Yoo, S.Y.; Jeon, K.W.; Na, H.S.; Lee, Y.L.; Jeong, D.W.; Bae, J.W.; Nah, I.W.; et al. Key properties of Ni-MgO-CeO_2, Ni-MgO-ZrO_2, and Ni-MgO-Ce(1-x)Zr(x)O_2 catalysts for the reforming of methane with carbon dioxide. *Green Chem.* **2018**, *20*, 1621–1633. [CrossRef]
32. Bore, M.T.; Pham, H.N.; Ward, T.L.; Datye, A.K. Role of pore curvature on the thermal stability of gold nanoparticles in mesoporous silica. *Chem. Commun.* **2004**, *22*, 2620–2621. [CrossRef]
33. Wang, E.; Yang, F.; Song, M.; Chen, G.; Zhang, Q.; Wang, F.; Bing, L.; Wang, G.; Han, D. Recent advances in the unsupported catalysts for the hydrodesulfurization of fuel. *Fuel Process. Technol.* **2022**, *235*, 107386. [CrossRef]
34. Cervantes, J.A.M.; Huirache-Acuña, R.; de León, J.N.D.; Moyado, S.F.; Cruz-Reyes, J.; Alonso-Núñez, G. Unsupported CoNixMo sulfide hydrodesulfurization catalysts prepared by the thermal decomposition of trimetallic tetrabutylammonium thiomolybdate: Effect of nickel on sulfur removal. *React. Kinet. Mech. Catal.* **2020**, *131*, 187–198. [CrossRef]
35. Bernard, P.; Stelmachowski, P.; Broś, P.; Makowski, W.; Kotarba, A. Demonstration of the Influence of Specific Surface Area on Reaction Rate in Heterogeneous Catalysis. *J. Chem. Educ.* **2021**, *98*, 935–940. [CrossRef]
36. Marafi, M.; Stanislaus, A.; Furimsky, E. *Handbook of Spent Hydroprocessing Catalysts*, 2nd ed.; Elsevier: Amsterdam, The Netherlands, 2017.
37. Zhang, M.; Wang, C.; Wang, K.; Han, Z.; Bello, S.S.; Guan, G.; Abudula, A.; Xu, G. Gentle hydrotreatment of shale oil in fixed bed over Ni-Mo/Al_2O_3 for upgrading. *Fuel* **2020**, *281*, 118495. [CrossRef]
38. Cai, B.; Zhou, X.C.; Miao, Y.C.; Luo, J.Y.; Pan, H.; Huang, Y.B. Enhanced catalytic transfer hydrogenation of ethyl levulinate to γ-valerolactone over a robust Cu-Ni bimetallic catalyst. *ACS Sustain. Chem. Eng.* **2017**, *5*, 1322–1331. [CrossRef]
39. Biswas, P.; Narayanasarma, P.; Kotikalapudi, C.M.; Dalai, A.K.; Adjaye, J. Characterization and activity of ZrO_2 doped SBA-15 supported NiMo catalysts for HDS and HDN of bitumen derived heavy gas oil. *Ind. Eng. Chem. Res.* **2011**, *50*, 7882–7895. [CrossRef]
40. Kobayashi, K.; Nagai, M. Active sites of sulfided NiMo/Al_2O_3 catalysts for 4,6-dimethyldibenzothiophene hydrodesulfurization-effects of Ni and Mo components, sulfidation, citric acid and phosphate addition. *Catal. Today* **2017**, *292*, 74–83. [CrossRef]
41. Liu, Z.; Han, W.; Hu, D.; Sun, S.; Hu, A.; Wang, Z.; Jia, Y.; Zhao, X.; Yang, Q.; Ni, E.O.; et al. Effects of Ni–Al_2O_3 interaction on NiMo/Al_2O_3 hydrodesulfurization catalysts. *J. Catal.* **2020**, *387*, 62–72. [CrossRef]
42. Vakros, J.; Bourikas, K.; Kordulis, C.; Lycourghiotis, A. Influence of the impregnation pH on the surface characteristics and the catalytic activity of the Mo/γ-Al_2O_3 and CoMo/γ-Al_2O_3 hydrodesulfurization catalysts prepared by equilibrium deposition filtration (EDF). *J. Phys. Chem. B.* **2003**, *107*, 1804–1813. [CrossRef]
43. Wang, X.; Zhao, Z.; Zheng, P.; Chen, Z.; Duan, A.; Xu, C.; Jiao, J.; Zhang, H.; Cao, Z.; Ge, B. Synthesis of NiMo catalysts supported on mesoporous Al_2O_3 with different crystal forms and superior catalytic performance for the hydrodesulfurization of dibenzothiophene and 4,6-dimethyldibenzothiophene. *J. Catal.* **2016**, *344*, 680–691. [CrossRef]
44. Gutiérrez, O.Y.; Klimova, T. Effect of the support on the high activity of the (Ni)Mo/ZrO_2-SBA-15 catalyst in the simultaneous hydrodesulfurization of DBT and 4,6-DMDBT. *J. Catal.* **2011**, *281*, 50–62. [CrossRef]

45. Yan, S.; Su, F.; Wang, X.; Yao, Z.; Liu, J. The mechanism of additives to unsupported Ni-Mo hydrodesulphurization catalyst. *IOP Conf. Ser. Earth Environ. Sci.* **2020**, *474*, 052008. [CrossRef]
46. Liu, Z.; Han, W.; Hu, D.; Nie, H.; Wang, Z.; Sun, S.; Deng, Z.; Yang, Q. Promoting effects of SO42-on a NiMo/γ-Al_2O_3hydrodesulfurization catalyst. *Catal. Sci. Technol.* **2020**, *10*, 5218–5230. [CrossRef]
47. Brito, J.L.; Laine, J.; Pratt, K.C. Temperature-programmed reduction of Ni-Mo oxides. *J. Mater. Sci.* **1989**, *24*, 425–431. [CrossRef]
48. Zhou, T.N.; Yin, H.L.; Liu, Y.Q.; Han, S.N.; Chai, Y.M.; Liu, C.G. Effect of phosphorus content on the active phase structure of NiMo/Al_2O_3 catalyst. *Ranliao Huaxue Xuebao/J. Fuel Chem. Technol.* **2010**, *38*, 69–74. [CrossRef]
49. Ríos-Caloch, G.; Santes, V.; Escobar, J.; Valle-Orta, M.; Barrera, M.C.; Hernandez-Barrera, M. Effect of chitosan addition on NiMo/Al_2O_3 catalysts for dibenzothiophene hydrodesulfurization. *Int. J. Chem. React. Eng.* **2012**, *10*. [CrossRef]
50. Rollmann, L.D. Systematics of shape selectivity in common zeolites. *J. Catal.* **1977**, *47*, 113–121. [CrossRef]
51. Spence, J.A.; Vahrman, M. Aliphatic hydrocarbons in a low-temperature tar. *J. Appl. Chem.* **1967**, *17*, 143–146. [CrossRef]
52. Ahmed, D.J.; Al-Abdaly, B.I.; Hussein, S.J. Synthesis and Characterization of New nano catalyst Mo-Ni/TiO_2-γAl_2O_3 for Hydrodesulphurization of Iraqi Gas Oil. *Baghdad Sci. J.* **2021**, *18*, 1557–1567. [CrossRef]
53. Zhou, J.; Hua, Z.; Liu, Z.; Wu, W.; Zhu, Y.; Shi, J. Direct synthetic strategy of mesoporous ZSM-5 zeolites by using conventional block copolymer templates and the improved catalytic properties. *ACS Catal.* **2011**, *1*, 287–291. [CrossRef]
54. Ahn, S.Y.; Kim, K.J.; Kim, B.J.; Shim, J.O.; Jang, W.J.; Roh, H.S. Unravelling the active sites and structure-activity relationship on Cu–ZnO–Al_2O_3 based catalysts for water-gas shift reaction. *Appl. Catal. B Environ.* **2023**, *325*, 122320. [CrossRef]
55. Wang, B.; Zhao, Z.; Xiao, C.; Li, P.; Zhao, Z.; Xu, C.; Meng, Q.; Li, J.; Duan, A.; Chen, Z. Hydrotreating Performance of FCC Diesel and Dibenzothiophene over NiMo Supported Zirconium Modified Al-TUD-1 Catalysts. *Ind. Eng. Chem. Res.* **2018**, *57*, 11868–11882. [CrossRef]